Invited Paper

Tailored light fields: Nondiffracting and self-similar beams for optical structuring and organization

C. Alpmann*, M. Boguslawski, P. Rose, M. Woerdemann, C. Denz
Institute of Applied Physics and Center for Nonlinear Science (CeNoS), University of Muenster
Corrensstraße 2/4, 48149 Münster, Germany

ABSTRACT

Microscopic structuring and organization of matter utilizing optically induced forces has a high potential to enable novel material properties and photonic features. We briefly review two promising classes of light fields that combine a high degree of order with exciting propagation properties, and demonstrate applications in optical micromanipulation and the creation of refractive index gratings in photorefractive materials. While the class of nondiffracting beams allows for axially extended optical potential landscapes and corresponding structuring of the refractive index, the class of self-similar beams offers continuous diffraction during propagation that can be exploited for two- and three-dimensional optical organization. We demonstrate how the transverse organization of the structured light fields can be transferred to corresponding structuring of bulk material and colloidal systems.

Keywords: Holographic beam shaping, optical micromanipulation, nondiffracting beams, Mathieu beams, Ince Gaussian beams, structured light fields, photonic lattices, optical induction

1. INTRODUCTION

The fundamental Gaussian beam, being the typical output of optical resonators, is the basis of the vast majority of laser experiments. Even if certain complex intensity or phase distributions, polarization, momentum and propagation properties are required, the fundamental Gaussian beam often is the basis for subsequent conversion to higher order modes. Because beam shaping has been a field of interest since the invention of the laser, several mechanical, electro-optic, acousto-optic, and holographic modulation techniques have been developed. Today, especially holographic modulation plays an important role, because it enables almost arbitrary beam shapes in real-time applications. During the history of complex light fields, the families of Hermite–Gaussian (HG) and Laguerre–Gaussian (LG) beams have been of unequaled importance, as they are typical eigenmodes of optical laser resonators and can be generated with high efficiency. In applications as laser resonators, optical fibers or nonlinear photonics, particular solutions with stable propagation properties are of interest. HG as well as LG modes posses stable propagation properties because they are exact solutions to the paraxial Helmholtz equation. However, being solutions of the paraxial Helmholtz equation in transverse Cartesian and polar coordinates, respectively, they are limited to particular symmetries, constricting potential applications. With the class of Ince-Gaussian (IG) beams, a more general family of solutions in transverse elliptical coordinates has been introduced recently [1] which includes all HG and LG beams as limiting cases. For applications in optical micromanipulation which usually rely on fundamental Gaussian beams [2] or relatively simple holographic multiplexing of a discrete number of these beams [3], the IG beams offer a complementary approach. Instead of a number of individual optical potential wells, induced by the discrete beams, higher order modes with their complex and tunable structure can induce continuous optical potential landscapes, “tailored” to a specific application.

All Gaussian beams spread during propagation as can be easily observed with the fundamental Gaussian beam that features a position along the beam axis where the beam diameter is minimal, the beam waist, and unavoidably spreads while propagating further. This spreading is due to diffraction and cannot be avoided for fundamental optical reasons. Many applications, however, would benefit from a beam that does not spread or only spreads less during propagation. Two important examples, on which we will put a focus on in the following, are applications in optical micromanipulation

* c.alpmann@uni-muenster.de; phone +49 251 83-33542; fax +49 251 83 33513; www.nichtlineare-photonik.de

Complex Light and Optical Forces VI, edited by Enrique J. Galvez, David L. Andrews, Jesper Glückstad, Marat S. Soskin, Proc. of SPIE Vol. 8274, 82740R · © 2012 SPIE · CCC code: 0277-786X/12/$18 · doi: 10.1117/12.908903

when axially extended potential wells are desired and the induction of axially extended refractive index gratings in bulk photorefractive materials. Interestingly, there do exist solutions to the Helmholtz equation that are invariant during propagation. Approximations to these propagation-invariant light fields can be realized experimentally and usually are called "nondiffracting" beams. These beams feature transverse intensity distributions that remain unchanged in a central region close to the beam axis and do not spread when the light field propagates.

In the following we will briefly review basic concepts of nondiffracting and self-similar beams and present applications in the fields of optical micromanipulation of colloidal particles and induction of functional refractive index gratings in bulk photorefractive materials.

2. NONDIFFRACTING LIGHT FIELDS

2.1 General description

Every propagating electromagnetic wave is subject to the phenomena of diffraction and divergence. Nevertheless, there are beam classes that seem to ignore these physical properties and propagate diffraction-free over a certain distance [4]. They are denoted as nondiffracting beams. Their transverse intensity profile is produced by phase locked interference of plane waves, propagating on a cone surface. Thus it is possible that nondiffracting beams maintain both their structure and spatial extent during propagation (Figure 1 (a)). The individual interfering partial beams (plane waves) are still subject to divergence and show diffraction effects, fulfilling every physical law.

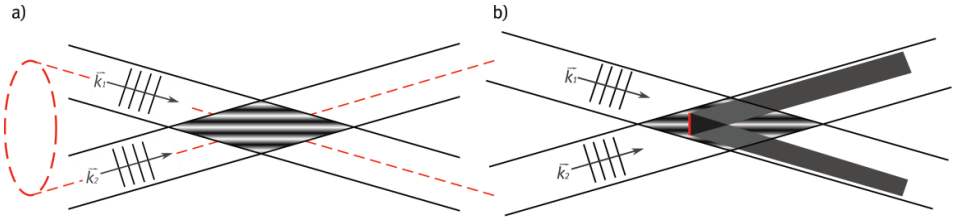

Figure 1 (a) Nondiffracting cosine beam as superposition of two plane waves propagating on a cone surface. (b) Self-healing effect after a beam distortion by an obstacle (red) within the nondiffracting area.

As solutions of the Helmholtz equation, nondiffracting beams can be separated into a transverse and a longitudinal part

$$\Psi(\vec{r}) = \Psi_t(r_1, r_2) \cdot e^{ik_z z}, \tag{1}$$

where the transverse field distribution Ψ_t is independent of the propagation variable z, as requested for nondiffracting beams. The simplest nondiffracting "beam" is obtained by the interference of two plane waves, resulting in a transverse cosine lattice, as depicted in Figure 1. This propagation invariant light field is not actually localized at the beam axis and thus the term "beam" might be unfavorable but with increasing number of constituting plane waves the degree of localization increases [5]. Depending on the symmetry, the Helmholtz equation can be transferred to different geometries, where it is at least separable in four different coordinate systems:

Cartesian coordinates:	Cosine beams
polar coordinates:	Bessel beams
elliptic coordinates:	Mathieu beams
parabolic coordinates:	Weber beams

Figure 2 shows a selection of intensity distributions of nondiffracting beams, illustrating column by column these four families of nondiffracting beams. The transverse extent and shape of each beam family depends on the corresponding symmetry, where as their propagation behavior is equal. Nondiffracting beams are obtained by phase-locked interference of plane waves placed on a ring in the Fourier space. The resulting quasi periodic transverse lattices are still propagation invariant and occur in nearly arbitrary integer-folded geometries. An infinite extension of the nondiffracting area, i.e. transverse and axial extent, of ideal nondiffracting beams would only be possible with infinite energy. But as this

condition cannot be fulfilled in any experimental implementation, nondiffracting beams always interfere in a finite volume, and thus result in a finite nondiffracting area.

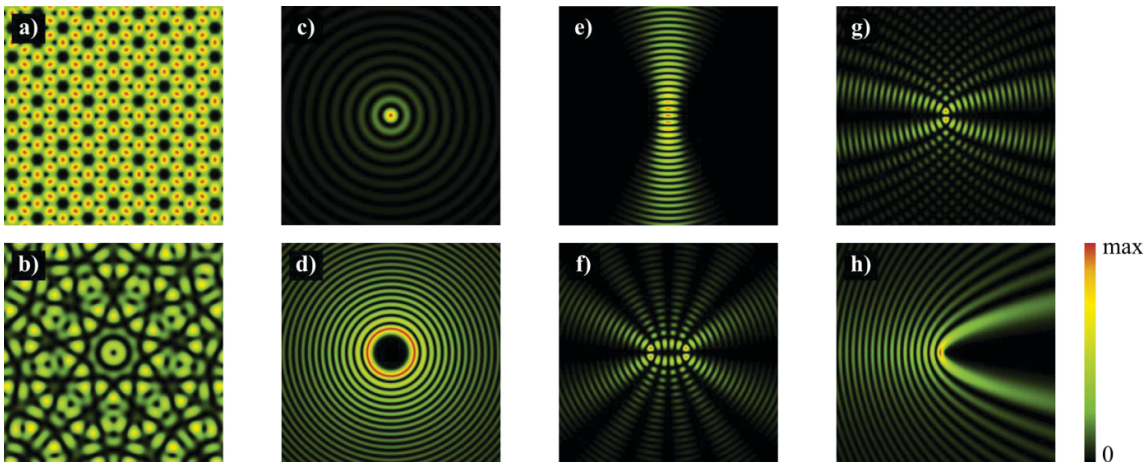

Figure 2 Selection of nondiffracting beams; Cosine beams: (a) Kagome beam, (b) nine-fold beam; Bessel beams: (c) of 0^{th} order, (d) of 10^{th} order; Mathieu beams: (e) 0^{th} order and even, (f) 6^{th} order and odd; Weber beams: (g) symmetric and (h) continuous.

An important property of nondiffracting beams, the so-called self-healing or self-reconstructing effect [6,7], originates from their geometry of interfering waves. It describes the complete reconstruction of the transverse beam profile after a certain propagation distance, when it has been previously affected by a (small) obstacle. As depicted in Figure 1(b) the beam is fully reconstructed during propagation behind the "shadow zone" of an obstacle within the nondiffracting area of the beam.

As the nondiffracting area results of a phase-locked interference of plane waves, all propagating on a cone surface, these waves are localized on a ring in the corresponding Fourier plane. All previously mentioned nondiffracting beams belong to the class of straight nondiffracting beams, meaning their transverse field distribution being perpendicular to the propagation direction, does not change during propagation. Beside these beams, the class of accelerating nondiffracting beams recently became popular. In particular Airy beams, which propagate on a curved trajectory arose high attention in the field of optical micro manipulation [8].

In the following, we will concentrate on straight nondiffracting beams and especially beams in elliptic geometries, as they provide a higher degree of flexibility because of the option to vary the eccentricity f of the coordinate system. In the case of $f = 0$ and $f = \infty$ polar and Cartesian coordinates are included, respectively.

2.2 Mathieu beams

The Helmholtz equation in elliptical coordinates can be reduced to a single-periodic differential equation, the Mathieu equation [9]

$$\left(\frac{\mathrm{d}^2}{\mathrm{du}^2} + (\mathrm{a} - 2\mathrm{q}\cos(2\mathrm{u}))\right)\mathrm{W}(\mathrm{u}) = 0. \qquad (2)$$

The equation depends on the ellipticity parameter $q = \frac{1}{4}f^2k_t^2$, proportional to the squares of the eccentricity of the elliptical coordinates f and the transverse wave vector k_t, and the separation constant a. From the classical theory of ordinary differential equations, the Mathieu equation always has two solutions: one even and one odd solution [9], being π or 2π periodic functions, known as the first order Mathieu functions.

The complete propagation invariant solutions of the Helmholtz equation are known as even and odd Mathieu beams of order m, each described by a product of two out of four Mathieu functions (Je_m, Jo_m, ce_m, se_m), the propagation term ($e^{ik_z z}$) and a time dependence ($e^{i\omega t}$):

$$\mathrm{M}_m^e(\eta,\xi,z,q) = C_m\, \mathrm{Je}_m(\xi,q)\mathrm{ce}_m(\eta,q)\, e^{ik_z z}\, e^{i\omega t}, \quad m = 0,1,2,3,\ldots\ , \tag{3}$$

$$\mathrm{M}_m^o(\eta,\xi,z,q) = S_m\, \mathrm{Jo}_m(\xi,q)\mathrm{se}_m(\eta,q)\ e^{ik_z z}\, e^{i\omega t}, \quad m = 1,2,3,\ldots\ , \tag{4}$$

where η and ξ are the elliptical coordinates and C_m and S_m normalizing constants. Figure 3 exemplarily shows a transverse and the two longitudinal intensity distributions of an even Mathieu beam of 0th order, illustrating the nondiffracting property.

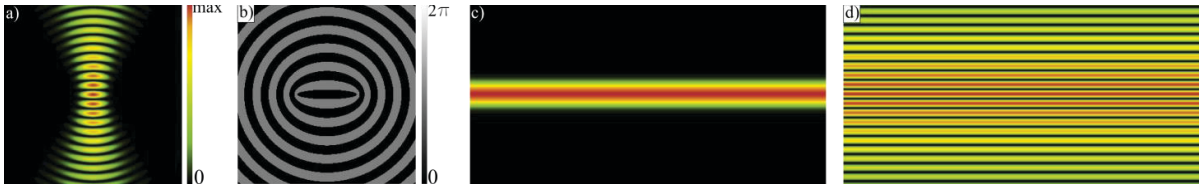

Figure 3 Nondiffracting even Mathieu beam of zeroth order: (a) transverse (xy-) intensity, (b) transverse phase, (c) xz-intensity, and (d) yz-intensity distribution.

Besides even and odd Mathieu beams, a superposition of both is known as *helical* Mathieu beams, as their higher modes are characterized by helical intensity distributions.

$$\mathrm{HM}_m^{\pm}(\eta,\xi,q) = \mathrm{M}_m^e(\eta,\xi,q) \pm i \cdot \mathrm{M}_m^o(\eta,\xi,q), \quad m = 0,1,2,3,\ldots \tag{5}$$

In contrast to even and odd Mathieu beams with discrete phase distributions of values $[0,\pi]$, helical Mathieu beams consist of continuous phase distributions.

Figure 4 shows a selection of even, odd and helical Mathieu beams. In the top row the normalized intensity distributions are given for different orders, indicating the variety of transverse field distributions of Mathieu beams. In the bottom row, the corresponding phase distributions are shown, indicating the difference between discrete phase distributions of even and odd Mathieu beams (a)-(e), compared to the continuous phase distributions of helical Mathieu beams in (f)-(g).

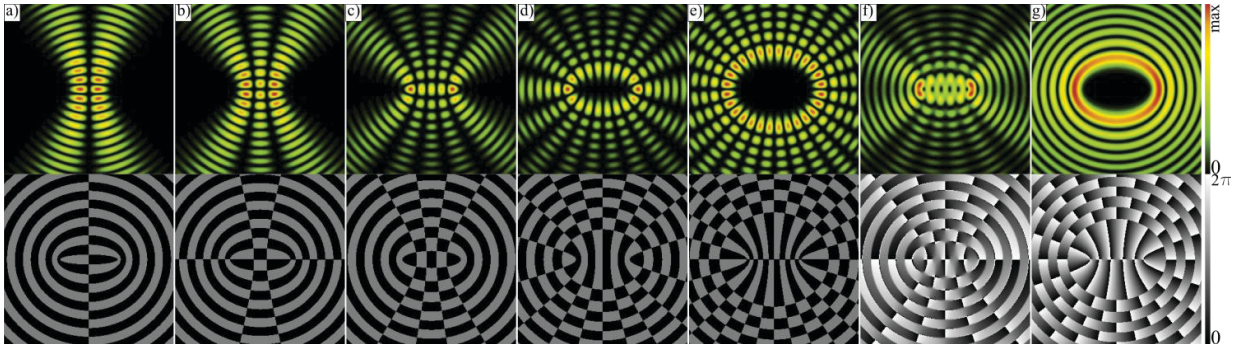

Figure 4 Selection of normalized intensity (top) and corresponding phase (bottom) distributions of even, odd and helical Mathieu beams (q=27). (a) M_1^e, (b) M_3^o, (c) M_4^e, (d) M_9^e, (e) M_{14}^o, (f) HM_6^+, (g) HM_{12}^+.

3. SELF-SIMILAR LIGHT FIELDS

3.1 General description

Self-similar beams are the most prominent class of laser beams as they are natural solutions to the resonator problem and hence widely available as output of commercial and research lasers. The fundamental Gaussian beam, as the typical single mode output of optical resonators, is the basis of most laser experiments. In contrast to nondiffracting beams, self-similar beams maintain their transverse shape during propagation, even in the far field, but scale due to divergence during free-space propagation. Mathematically they can be described as solutions of the paraxial Helmholtz equation, which is solvable in different geometries, similar to nondiffracting beams:

geometry:	**straight nondiffracting:**	**self-similar:**
Cartesian coordinates	Cosine beams	Hermite-Gaussian beams
polar coordinates	Bessel beams	Laguerre-Gaussian beams
elliptic coordinates	Mathieu beams	Ince-Gaussian beams

Self-similar beams offer a higher diversity of transverse field distributions, compared to nondiffracting beams, characterized by two parameters describing the order p and degree m of the individual mode. Despite their diversity, however, the vast majority of applications is still restricted to the fundamental Gaussian beam and other lower order Hermite-Gaussian or Laguerre-Gaussian beams. The recently found fundamental class of Ince-Gaussian modes offers significantly higher diversity of transverse beam profiles, as it is the general solution of the paraxial Helmholtz equation in elliptical coordinates because, with the eccentricity as a parameter, it includes Hermite-Gaussian and Laguerre-Gaussian beams. Thus in the following, we focus on Ince-Gaussian beams.

3.2 Ince-Gaussian beams

The paraxial Helmholtz equation in elliptical coordinates can be reduced to the Ince equation, given by [10]

$$\left(\frac{d^2}{du^2} + \epsilon \sin(2u)\frac{d}{du} + (a - p\epsilon\cos(2u))\right) W(u) = 0, \tag{6}$$

where ϵ denotes the ellipticity parameter $\epsilon = 2\mathrm{f}_0^2/\omega_0^2$, which is a function of the eccentricity of the elliptical coordinates f_0 and the beam waist ω_0, p and a denote separation constants.

The complete solutions of the paraxial Helmholtz equation in elliptical coordinates can be divided into two subgroups: even Ince-Gaussian and odd Ince-Gaussian beams:

$$\mathrm{IG}^e_{p,m}(\eta,\xi,z,\epsilon) = C \cdot \mathrm{C}^m_p(i\xi,\epsilon)\mathrm{C}^m_p(\eta,q)\, e^{ip\cdot\psi_\mathrm{G}(z)}\, \Psi_{\mathrm{Gauss}}, \tag{7}$$

$$\mathrm{IG}^o_{p,m}(\eta,\xi,z,\epsilon) = S \cdot \mathrm{S}^m_p(i\xi,\epsilon)S^m_p(\eta,q)\, e^{ip\cdot\psi_\mathrm{G}(z)}\, \Psi_{\mathrm{Gauss}}, \tag{8}$$

with the Ince functions $(\mathrm{C}^m_p, \mathrm{S}^m_p)$, a phase term $(e^{ip\cdot\psi_\mathrm{G}(z)})$ including an additional Gouy phase shift $(\psi_\mathrm{G}(z))$, the fundamental Gaussian beam (Ψ_{Gauss}), and normalizing constants C, S. In contrast to nondiffracting beams, self-similar modes are described by two parameters: the order p and degree m, highly increasing the number and variety of different transverse modes. The two parameter p and m always have the same parity.

Similar to nondiffracting beams, helical self-similar modes are given by the combination of even and odd modes:

$$\mathrm{HIG}^{\pm}_{p,m}(\eta,\xi,z,\epsilon) = \mathrm{IG}^e_{p,m}(\eta,\xi,z,\epsilon) \pm i \cdot \mathrm{IG}^o_{p,m}(\eta,\xi,z,\epsilon). \tag{9}$$

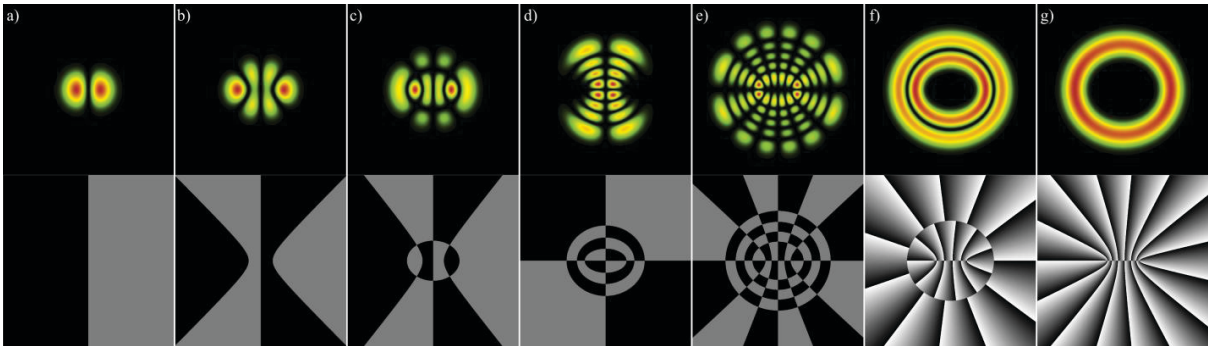

Figure 5 Selection of normalized intensity (top) and corresponding phase (bottom) distributions of even, odd and helical Ince-Gaussian beams ($\epsilon = 2$). (a) $\mathrm{IG}^e_{1,1}$, (b) $\mathrm{IG}^e_{3,3}$, (c) $\mathrm{IG}^e_{5,3}$, (d) $\mathrm{IG}^o_{8,2}$, (e) $\mathrm{IG}^o_{14,6}$, (f) $\mathrm{HIG}^+_{13,11}$, (g) $\mathrm{HIG}^+_{15,15}$ (color maps as before).

Figure 5 shows a small selection of typical even, odd and helical Ince-Gaussian modes, indicating their normalized intensities and corresponding phase distributions, respectively. As already mentioned with Mathieu beams, the helical modes of Ince-Gaussian beams are characterized by continuous phase distributions, compared to the discrete phase distributions of even and odd Ince-Gaussian beams.

After the introduction of nondiffracting and self-similar beams, we will concentrate on two fields of applications of these tailored light modes: optical micromanipulation and optical structuring of photorefractive material.

4. TAILORED OPTICAL TWEEZERS

Optical micromanipulation in the form of (holographic) optical tweezers is a well established tool with hundreds of applications in biology, medicine and physics. In the last decade especially the dynamic manipulation of multiple particles has been developed. The implementation of algorithms with low numerical effort as the lenses and gratings algorithm [11] and intuitive user interfaces made this field highly attractive to a wide range of research fields, wherefrom new applications with increasing demands arise and ask for new physical solutions. This progress currently results in a highly dynamic and widely spreading research field. Recent developments introduced complex light modes as a complementary approach to classical point traps, because they offer distinct advantages in the manipulation of non-spherical or functionalized particles [12,13].

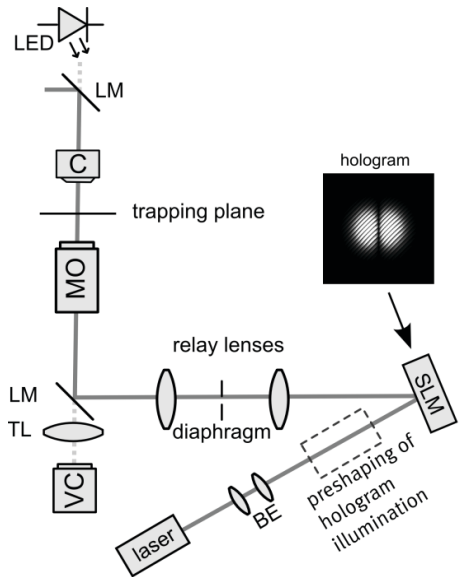

Figure 6 Experimental setup: Integration of complex optical light fields into a standard holographic optical tweezers setup. BE = beam expansion, C = condenser, LM = laserline mirror, MO = microscope objective, SLM = spatial light modulator, TL = tube lens, VC = video camera.

4.1 Generation of complex light fields in holographic optical tweezers

The generation of complex optical light fields in holographic optical tweezers is based on spatial light modulators (SLM). To maximize the available intensity in the trapping plane, the modulation efficiency should be as high as possible. Thus phase-only modulators are preferred where the complex field information (amplitude and phase) is encoded into a phase-only hologram. Different techniques have been proposed to calculate according holograms. The general concept that allows imprinting of amplitude information on a phase-only hologram employs a high frequency carrier grating which is modulated locally in such a way that it diffracts controlled amounts of light into one diffraction order [14]. Based on this basic concept, a number of variations have emerged that differ in the choice of the carrier grating type and frequency, the modulation function, or the utilized order of diffraction [14-22]

A standard holographic optical tweezers setup, as depicted by Figure 6, consists of a microscope and the integrated optical trapping beam. For practical reasons, the SLM is usually placed in a Fourier plane with respect to the trapping plane, requiring the phase holograms to be Fourier holograms of the desired trapping light field.

4.2 Generation of nondiffracting beams in optical tweezers and pre-shaping of the hologram illumination

Unfortunately, the field distribution of nondiffracting beams in the Fourier space consists of an (in the ideal case infinitesimally) narrow ring. For this reason, the modulation efficiency in general would be too low to allow for optical micromanipulation, where the trapping forces are proportional to the available intensity. To overcome this bottleneck, a pre-shaping technique for the hologram illumination can be employed [12]. The idea is to concentrate all available power in the area of interest, i.e. on a narrow ring, before the actual holographic modulation is performed. If the radial expansion of the field distribution in the Fourier plane is already given by the pre-shaped ring illumination, it is sufficient to use a Fourier-hologram calculated from the corresponding angular Mathieu functions (ce_m, se_m), as shown in Figure 7 (e)-(g). As pre-shaping element a conical lens (or a combination of two) can be realized either by refractive axicons or holographically by an SLM.

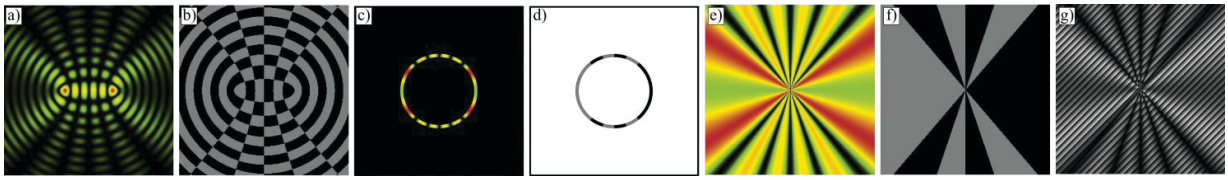

Figure 7 Fourier-hologram calculation of nondiffracting beams: 5th order even Mathieu beam (q=27). (a) normalized intensity, (b) phase, (c) normalized Fourier- intensity, (d) Fourier-phase, (e) angular Fourier-intensity, (f) angular Fourier-phase, (g) phase-only Fourier-hologram including intensity and phase information (color maps as before).

4.3 3d particle manipulation with nondiffracting Mathieu beams

Nondiffracting beams are a powerful tool in optical micromanipulation, as they provide axially expanded trapping potentials, which can be used to build three dimensional particle assemblies. Figure 8 shows the theoretical (left) and experimental (middle) intensity distribution of a 4th order Mathieu beam in an optical tweezers setup. The three dimensional images consist of discrete isosurface plots, visualizing areas of similar intensities. The combination of scattering, gradient and gravitational forces allows stable trapping of e.g. silica spheres in the main intensity maxima, as illustrated on the right in Fig. 8. The particles can be stacked in the direction of light propagation because of the nondiffracting and self-healing beam properties [12]. Up to 6-7 stacked particles have been observed. The actual number depends on the ratio of particle radius and the expanded Rayleigh length of the beam. Besides trapping of spheres, the transverse intensity distribution of Mathieu beams allows to orient elongated particles with their long axis perpendicular to the propagation direction of the light [12]. Even stacking of orientated elongated particles becomes possible. This feature gives a new tool for the optical manipulation of rod shaped bacteria or nanorods, for example. The particle orientation and stereoscopic observation has been realized in cooperation with the University of Glasgow [12]

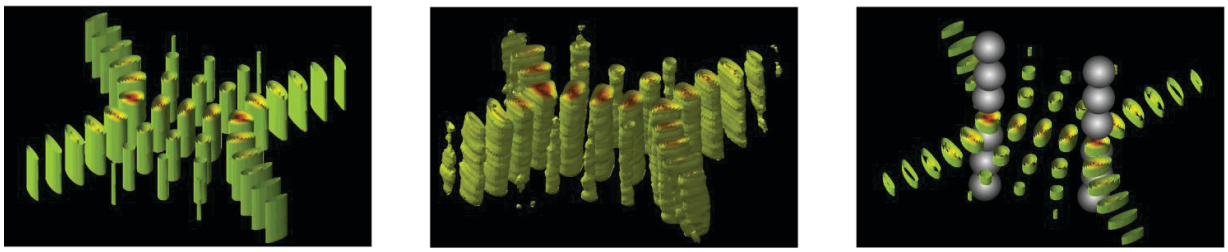

Figure 8 Three dimensional isosurface plots, visualizing light moulds of Mathieu beams, used for optical micromanipulation: Theoretical (left) and experimental (middle) intensity distributions of an even 4th order Mathieu beam; illustration of a possible three dimensional particle assembly (right).

4.4 Generation of self-similar Ince-Gaussian beams in optical tweezers

The generation of self-similar beams in holographic optical tweezers takes less computational effort than the generation of nondiffracting beams, as because of their self-similarity there is no need to calculate special Fourier-holograms. To use standard phase-only modulators, a blazed grating is weighted with the amplitude information and added to the corresponding phase distribution, as already introduced for nondiffracting beams. Figure 9 gives a selection of experimental results of Ince-Gaussian beams generated with this method. It can be seen, that a high modulation quality is achievable.

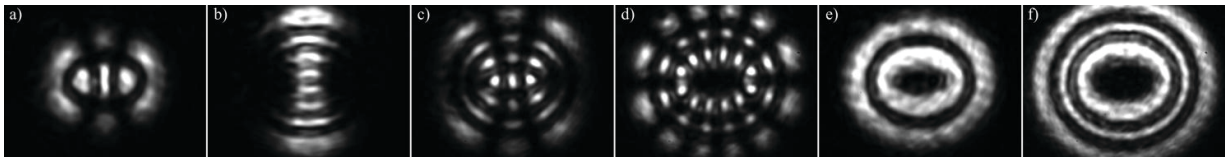

Figure 9 Experimental generation of Ince-Gaussian beams: (a) $IG_{4,2}^{e}$, (b) $IG_{7,1}^{o}$, (c) $IG_{8,2}^{e}$, (d) $IG_{10,6}^{o}$, (e) $HIG_{7,5}^{+}$, (f) $HIG_{12,8}^{+}$

Recently the manipulation of matter with Ince-Gaussian beams in optical tweezers has been demonstrated [13], which offers an amount of new trapping potentials for possible applications in optical micromanipulation. Figure 10 shows the organization of 1.5 µm Silica spheres in different configurations of even and odd Ince-Gaussian beams.

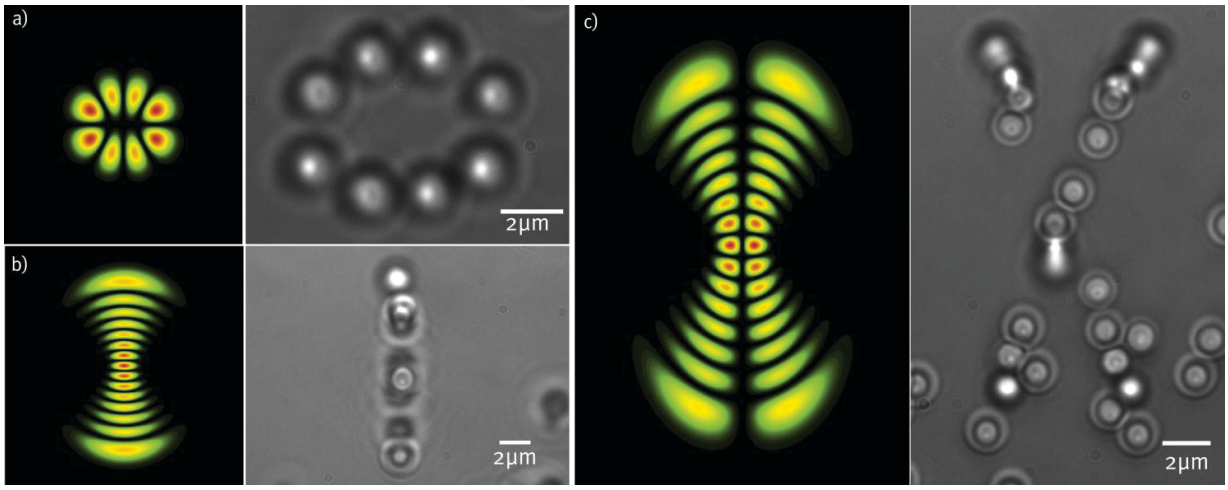

Figure 10 Particle manipulation with Ince-Gaussian beams demonstrated by the organization of 1.5 µm Silica spheres. (a) $IG^{o}_{4,4}$, (b) $IG^{e}_{14,0}$, (c) $IG^{e}_{15,1}$.

In Figure 10 (a) eight silica spheres are organized within the optical potential of an $IG^{o}_{4,4}$-beam, where one sphere is placed in each of the eight intensity peaks. By shifting the trapping plane in propagation direction, the relation of beam width and particle radius can be influenced. In (b) several spheres are trapped within an $IG^{e}_{14,0}$-beam, where the particles resemble the outer form of the beam, rather than occupying each individual intensity maximum. Besides the organization and trapping of particles in self-similar beams, the phenomenon of optical binding has been observed, as shown in Fig. 10 (c). All these examples demonstrate the possibility of self-similar Ince-Gaussian beams to be used in optical micromanipulation. In combination with their high diversity of transverse field distributions, they will become interesting for applications in many fields of material structuring, organization and manipulation.

5. OPTICAL STRUCTURING OF PHOTOREFRACTIVE MEDIA USING NONDIFFRACTING MATHIEU BEAMS

In the photonic research field, photonic structures offer an intriguing possibility of engineering, guiding and controlling the propagation of light by light itself [24,25]. Fascinating nonlinear phenomena of light propagation such as discrete soliton trains, vortex solitons as well as Bloch oscillation and Zener tunneling may be the basement of future techniques to route and process data in a photonic manner. Several methods have been carried out to develop particularly modulated refractive index structures, among them direct laser writing [26], (holographic) lithography [27], as well as the optical induction of photonic structures [28,29].

5.1 Principle of optical induction to create photonic structures

Implementations of the latter technique offer the significant advantage to reversibly generate light-induced refractive index distributions in low-intensity regimes provided by the electro-optic properties of a photorefractive medium [30]. Such specific media, for instance cerium doped strontium barium niobate (SBN:Ce) crystals, change their refractive index locally according to the intensity distribution of the illuminating light field (lattice beam), whereupon in particular for this kind of crystal the linear polarization state of the light determines the strength of the interplay between refractive index structure and lattice beam. Using a beam with a polarization perpendicular (s-polarization) to the symmetry axis of the crystal (c-axis), the electro-optical coefficient is small compared to the coefficient which is relevant for parallel polarization (p-polarization). Hence, to optically induce a refractive index structure one uses s-polarized lattice beams in combination with an external electrical field applied parallelly to the c-axis. For this configuration the effect of the

induced refractive index on the lattice beam itself is negligible. However, a probing beam is commonly p-polarized where the index modulation significantly manipulates the light propagation and in combination with high intensities the focusing or defocusing behavior given by the kind of nonlinearity becomes relevant [29].

5.2 Technical implementation of optical induction

To build up two-dimensionally modulated photonic structures we employ nondiffracting wave fields, utilizing their property of a translation invariant intensity distribution in direction of propagation connected with a transversely modulated intensity. Using the setup shown in Figure 11, nondiffracting beams can be formed which are longitudinally expanded over several centimeters, meeting a transverse structural size of tens of micrometers [31]. These particular interference fields in turn enable the optical induction of macroscopically elongated photonic structures with a transverse refractive index modulation on microscales.

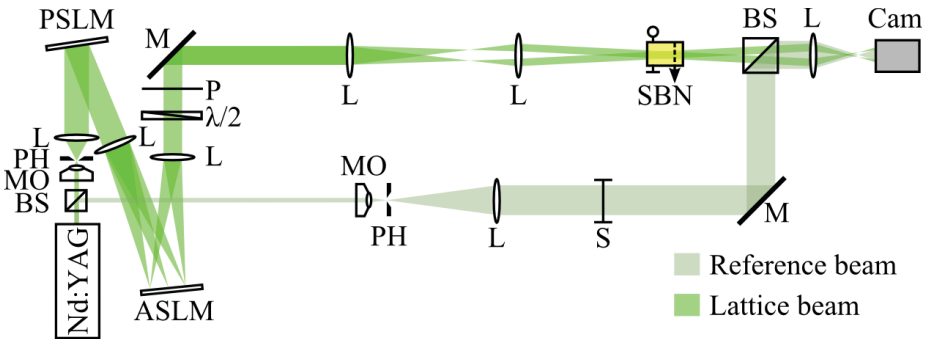

Figure 11 Experimental setup to optically induce and analyze photonic structures; A/PSLM: amplitude/phase manipulating spatial light modulator, Cam: camera, BS: beam splitter, L: lens, λ/2: half-wave plate, M: mirror, MO: microscope objective, P: polarizer, PH: pinhole, S: shutter, SBN: strontium barium niobate crystal.

However, it is a question of numerical aperture of the imaging devices to bring the inducing light field into high spatial frequencies in Fourier space and hence to reach smaller structural sizes in the corresponding real space.

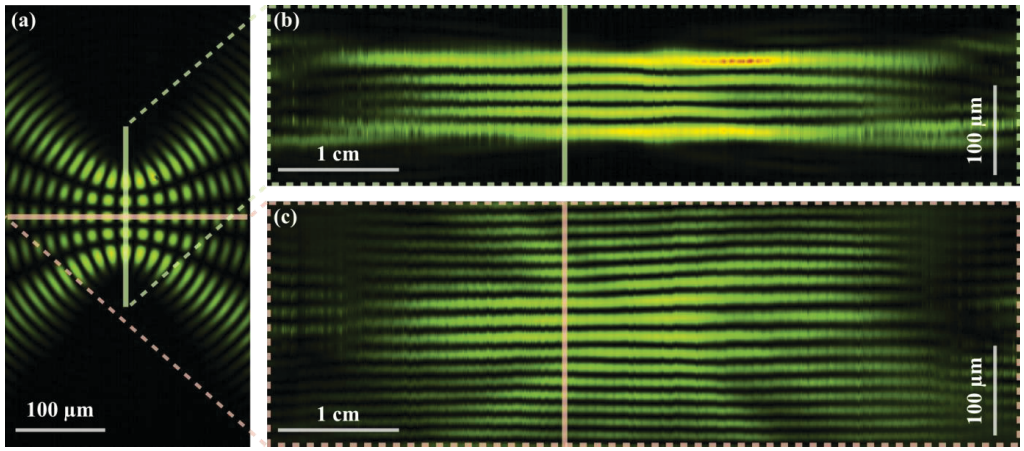

Figure 12 Analysis of the nondiffracting property of an even Mathieu beam of 4th order; (a) intensity distribution in a particular transverse plane perpendicular to direction of propagation; (b) and (c) development of the intensity along the propagation direction (horizontal) with respect to an orthogonal transverse direction (vertical), solid lines depict the respective position of the orthogonal planes, bars display the dimensions, where (b) and (c) are markedly stretched.

As similar to the generation of nondiffracting light fields for tweezers applications, the involvement of SLMs marks an enormous advantage in terms of dynamical and highly resolving computer controlled light field forming. Therefore, we implemented a phase modulator to influence the complex amplitude of an incoming plane wave and to experimentally create the desired wave field, as already described above. In contrast to tweezers experiments, the beam shaping plane of

these experiments (position of the PSLM) reveals a direct rather than a Fourier relation to the working area (trapping plane or crystal position, respectively), where the actual experiment takes place. Subsequently, the modulated light field is additionally Fourier filtered by means of an amplitude modulator blocking all spatial frequencies except the required ones lying on a ring in the Fourier plane. A telescope with a magnification factor of approximately 0.15 images the formed wave field into the SBN crystal, ensuring that the interference volume longitudinally exceeds the crystal length of 50mm.

For analysis, we installed a lens and a camera onto a translation stage in such a way that the imaging plane in real space can be shifted longitudinally. In this manner, we are able to analyze the light field by recording its transverse intensity distributions over a length of 10 cm. Stacking of equivalent rows or lines of transverse intensities according to several propagation positions allows us to determine the development of the intensity with increasing propagation distance. Figure 12 depicts three intensity distributions of a nondiffracting Mathieu wave field with even symmetry and 4th order in particular mutual orthogonal planes: positioned (a) transversely, and (b), (c) along the propagation direction, where the light propagates horizontally and the respective transverse coordinate is depicted vertically.

Additionally, we implemented a reference beam in terms of analyzing the field's phase distribution via digital-holography techniques [32]. On the one hand, we can thus determine the correct creation of the nondiffracting wave field by receiving the information of intensity and phase. On the other hand, the fixed phase of the reference beam allows us to directly depict the phase retardation of a probing plane wave propagated through the structured SBN crystal, which is the basic principle of a two-dimensionally resolved refractive index measurement [33].

5.3 Creation of refractive index lattices

Based on the shown optical-induction setup, in the following several experimental results of generated photonic structures in elliptic symmetries are presented. The set of implemented Mathieu beams shows a wide structural spectrum.

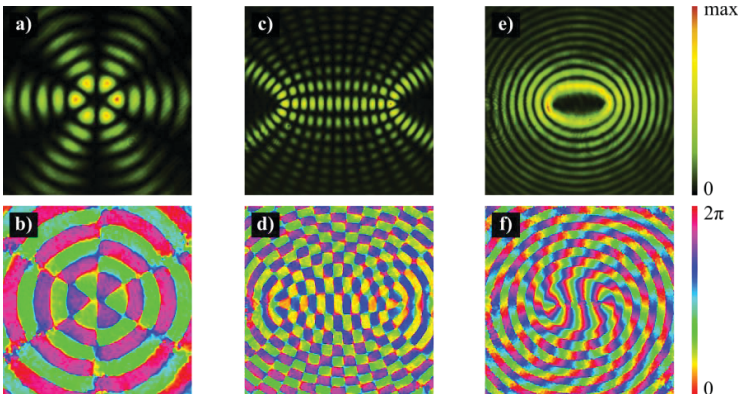

Figure 13 Amplitude (upper row) and phase distributions (lower row) of several Mathieu beams: (a)-(b) M_3^e; (c)-(d) M_{12}^e; (e)-(f) HM_8^+.

In Figure 13 intensity (upper row) and phase distributions (lower row) are shown for three different Mathieu beams. In detail, the first beam of the 3rd order reveals an even transverse field distribution and is further characterized by an eccentricity parameter f = 0.1, shown in the left column of Figure 13. The second beam holds also an even symmetry and has the order 12 with f = 1.5, depicted in the middle column. A superposition of an even and odd Mathieu beam, forming a helical beam shape, is depicted in the right column of Figure 13. In contrast to the phase pictures of the two first Mathieu beams, this third beam reveals a continuous phase rather than areas of equal-valued phases.

Each presented Mathieu beam was used to optically induce photonic structures in elliptic symmetries, as the results are depicted in Figure 14. The intensity at the back face of the SBN crystal of a probe wave propagated through the induced structure is shown in the upper row, whereupon the lower row depicts the phase retardation of the probe beam, resembling the induced photonic structure. All characteristic symmetries of the inducing beams can be found in the analytical pictures of Figure 14, which proof a successful optical induction of the desired photonic structures. However, the inherent modulation anisotropy of the SBN crystal [30] causes a strong index modulation in horizontal direction (parallel to c-axis) and a weak modulation perpendicular to the c-axis. Especially the photonic structure induced by the helical beam [cf. Figure14 (e) and (f)] depicts this effect impressively.

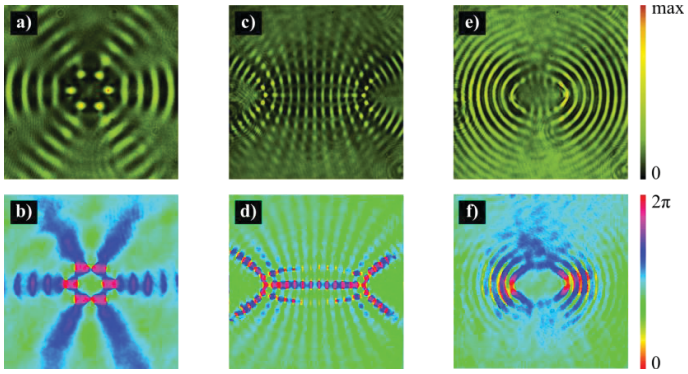

Figure 14 Analysis results of optically induced photonic structures in elliptic symmetry; upper row depicts the intensity and lower row the local phase retardation of a plane probe beam (offset); inducing beams are according to the columns of Figure 13.

6. CONCLUSION

Tailored optical light fields are characterized by a diversity of transverse field distributions in combination with stable propagation properties. In this article, we introduced and compared two fundamental beam classes: nondiffracting and self-similar light beams. Both exist in different geometries and thus offer a variety of beam shapes. Besides a general description, we focused on elliptical beams, as they are the more general solutions and include Cartesian and polar beams as special cases. We have shown the potential of nondiffracting Mathieu beams for three dimensional material organization in optical tweezers applications and their potential for refractive index structuring in photorefractive materials. Additionally to nondiffracting beams, we focused on self-similar Ince-Gaussian beams and demonstrated their application in optical micromanipulation. Here two dimensional organization of silica spheres in different configurations and the phenomenon of optical binding have been shown. Concluding we state that both, nondiffracting and self-similar, beams offer a variety of field distributions compared with stable but different propagation properties. These differences on the one hand imply special demands for the generation of these light fields, but on the other hand facilitate their implementation in nearly all kind of laser applications.

ACKNOWLEDGEMENT

This work was partially supported by the DFG Grant No. TRR61.

REFERENCES

[1] Bandres, M.A. and Gutierrez-Vega, J.C., “Ince Gaussian beams”, Opt. Lett. 29(2), 144–146 (2004).
[2] Ashkin, A. Dziedzic, J.M. Bjorkholm, J.E. and Chu, S., “Observation of a single-beam gradient force optical trap for dielectric particles”, Opt. Lett. 11(5), 288–290 (1986).
[3] Woerdemann, M., Glaesener, S., Hoerner, F., Devaux, A., De Cola, L. Denz, C., “Dynamic and Reversible Organization of Zeolite L Crystals Induced by Holographic Optical Tweezers”, Adv. Mat. 22(37), 4176 (2010).
[4] Durnin, J., Miceli, J.J., and Eberly, J.H., “Diffraction-free beams”, Phys. Rev. Lett. 58(15), 1499–1501 (1987).
[5] Boguslawski, M., Rose, P., and Denz, C., “Increasing the structural variety of discrete nondiffracting wave fields”, Phys. Rev. A 84(1), 013832 (2011)
[6] Bouchal, Z., Wagner, J. and Chlup, M., “Self-reconstruction of a distorted nondiffracting beam”, Opt. Commun. 151(4), 207–211 (1998).
[7] Thomson, L.C. and Courtial, J., “Holographic shaping of generalized self-reconstructing light beams”, Opt. Commun. 281(5), 1217–1221 (2008).

[8] Baumgartl, J., Mazilu, M., and Dholakia, K., "Optically mediated particle clearing using Airy wavepackets", Nat. Phot. 2(11), 675–678 (2008).
[9] Arscott, F.M., "Two-parameter eigenvalue problems in differential equations", Proc. London Math. Soc. 3(14), 459–70 (1963).
[10] Ince, E.L., "A linear differential equation with periodic coefficients", Proc. London Math. Soc. 23, 56–74 (1923).
[11] Liesener, J., Reicherter, M., Haist, T., and Tiziani, H.J., "Multi-functional optical tweezers using computer-generated holograms", Opt. Commun. 185(1), 77 – 82 (2000).
[12] Alpmann, C., Bowman, R., Woerdemann, M., Padgett, M., and Denz, C., "Mathieu beams as versatile light moulds for 3d micro particle assemblies", Opt. Express 18(25), 26084–26091 (2010).
[13] Woerdemann, M., Alpmann, C. and Denz, C., "Optical assembly of microparticles into highly ordered structures using Ince–Gaussian beams", Appl. Phys. Lett. 98(11), 111101 (2011).
[14] Kirk, J., and Jones, A., "Phase-only complex-valued spatial filter", J. Opt. Soc. Am. 61, 1023–1028 (1971).
[15] Arrizón, V., Ruiz, U., Carrada, R., and González, L., "Pixelated phase computer holograms for the accurate encoding of scalar complex fields", J. Opt. Soc. Am. A 24, 3500–3507 (2007).
[16] Arrizón, V., Sanchez de-la Llave, D., Ruiz, U. and Mendez, G., "Efficient generation of an arbitrary nondiffracting Bessel beam employing its phase modulation", Opt. Lett. 34(9), 1456–1458 (2009).
[17] Bentley, J.B., Davis, J.A., Bandres, M.A., and Gutierrez-Vega, J.C., "Generation of helical Ince-Gaussian beams with a liquid-crystal display", Opt. Lett. 31(5), 649–651 (2006).
[18] Davis, J.A., Cottrell, D.M., Campos, J., Yzuel, M.J., and Moreno, I., "Encoding amplitude information onto phase-only filters", Appl. Opt. 38(23), 5004–5013 (1999).
[19] Davis, J.A., Cottrell, D.M., Campos, J., Yzuel, M.J., and Moreno, I., "Bessel function output from an optical correlator with a phase-only encoded inverse filter", Appl. Opt. 38(32), 6709–6713 (1999).
[20] Davis, J.A., Mitry, M.J., Bandres, M.A., Ruiz, I., McAuley, K.P., Cottrell, D.M., "Generation of accelerating Airy and accelerating parabolic beams using phase-only patterns", Appl. Opt. 48(17), 3170–3176 (2009).
[21] Lopez-Mariscal, C. and Gutierrez-Vega, J.C., "The generation of nondiffracting beams using inexpensive computer-generated holograms", Am. J. o. Phys. 75(1), 36–42 (2007).
[22] Roichman, Y., "Extended optical traps by shape-phase holography", US patent, US7 491 928 B2 (2009).
[23] Schonbrun, E., Piestun, R., Jordan, P., Cooper, J., Wulff, K., Courtial, J., and Padgett, M., "3d interferometric optical tweezers using a single spatial light modulator", Opt. Express 13(10), 3777–3786 (2005).
[24] Fleischer, J., Bartal, G., Cohen, O., Schwartz, T., Manela, O., Freedman, B., Segev, M., Buljan, H., and Efremidis, N.K., "Spatial photonics in nonlinear waveguide arrays", Opt. Express 13(6), 1780–1796 (2005).
[25] Lederer, F., Stegeman, G.I., Christodoulides, D.N., Assanto, G., Segev, M., and Silberberg, Y., "Discrete solitons in optics", Phys. Lett. 463(1), 1–126 (2008).
[26] Maruo, S., Nakamura, O., and Kawata, S., "Three-dimensional microfabrication with two-photon-absorbed photopolymerization", Opt. Lett. 22(2), 132–134 (1997).
[27] Berger, V., Gauthier-Lafaye, O., and Costard, E., "Photonic band gaps and holography", J. of Appl. Phys. 82(1), 60–64 (1997).
[28] Efremidis, N.K., Sears, S., Christodoulides, D.N., Fleischer, J.W., and Segev, M., "Discrete solitons in photorefractive optically induced photonic lattices", Phys. Rev. E 66(4), 046602 (2002).
[29] Fleischer, J.W., Segev, M., Efremidis, N.K., and Christodoulides, D.N., "Observation of two-dimensional discrete solitons in optically induced nonlinear photonic lattices", Nature 422(6928), 147–150 (2003).
[30] Desyatnikov, A.S., Neshev, D.N., Kivshar, Y.S., Sagemerten, N., Träger, D., Jägers, J., Denz, C., and Kartashov, Y.V., "Nonlinear photonic lattices in anisotropic nonlocal self-focusing media", Opt. Lett, 30(8), 869–871 (2005).
[31] Rose, P., Boguslawski, M., and Denz, C., "Nonlinear lattice structures based on families of complex nondiffracting beams", ArXiv e-prints, arXiv:1111.5543v1 (2011).
[32] Schnars, U. and Jüptner, W.P.O., "Digital recording and numerical reconstruction of holograms", Measurement Science and Technology 13(9), R85 (2002).
[33] Jian-Lin, Z., Peng, Z., Jian-Bo, Z. De-Xing, Y., Dong-Sheng, Y. and En-Pu, L., "Visualizations of light-induced refractive index changes in photorefractive crystals employing digital holography", Chinese Physics Letters 20(10), 1748 (2003).